Advances in Science and Technology Research Journal

Advances in Science and Technology Research Journal, 2025, 19(10), 252–264
https://doi.org/10.12913/22998624/208015
ISSN 2299-8624, License CC-BY 4.0

Received: 2025.05.08
Accepted: 2025.08.15
Published: 2025.09.01

Nonlinear free vibration analysis of skew functionally graded plate using novel shear deformation theory

Jitendra Singh[1], Ajay Kumar[1], Jacek Góra[2*], Wojciech Piasta[3]

[1] Department of Civil Engineering, National Institute of Technology Patna, Patna-800005, India
[2] Faculty of Civil Engineering and Architecture, Lublin University of Technology; Nadbystrzycka 40, 20-618 Lublin, Poland
[3] Faculty of Civil Engineering and Architecture, Kielce University of Technology; Al. Tysiąclecia PP 7, 25-314 Kielce, Poland
* Corresponding author's e-mail: j.gora@pollub.pl

ABSTRACT

The geometric nonlinearity-based free vibration analysis of shear deformable functionally graded material (FGM) plates is investigated in this paper. The nonlinear finite element equations are derived from hybrid hyperbolic higher-order shear deformation theory (HSDT). The Green–Lagrange nonlinear strain–displacement relation is incorporated in the formulation, along with all higher-order nonlinear strain terms to account for the geometric non-linearity developed during analysis. Typically, the constituent isotropic ceramic and metal phases follow a simple power-law distribution with the composition varying gradually with plate thickness. By adopting traction-free boundary conditions on the top and bottom faces of the plate, the fundamental equations are derived using a variational approach. An efficient C^0 continuity finite element formulation with 7 degrees of freedom (DOFs) per node is developed using homemade MATLAB code to produce the fundamental frequency and mode shape results. To prove the efficacy of the current model, convergence tests are conducted and the results are validated with existing literature. Parametric studies are performed for varied thickness ratios, aspect ratios, skewness of the plate, and volume fraction index with different boundary conditions, the fluctuation of nonlinear frequency ratio with amplitude ratio is highlighted.

Keywords: functionally graded plates, shear deformation plate theory, nonlinear free vibration analysis, geometric nonlinearity, finite element method.

INTRODUCTION

The behaviour of a plate with a large amplitude free flexural vibration (LAFFV) occurs in many technical applications, particularly in aeroplane panels. When a structure is deflected significantly, say half its thickness, it develops significant geometrical nonlinearity, owing to the formation of in-plane membrane stresses. The tensile nature of these membrane stresses stiffens the plate. The stiffening effect causes resonance frequencies to rise and mode shapes to change. As a result, the linear model is unable to fully predict the behaviour of the structures. As a result, in comparison to static large deflection behaviour of plates, geometrically nonlinear flexural vibration of plates has attracted a lot of interest in recent years. Functionally graded composites can perform modern and distinctive functions that conventional composite materials are unable to accomplish. These are advanced composite materials which are manufactured using powder metallurgy techniques from the combination of metal and ceramic, having microscopically inhomogeneous morphology. The FGM plate has a gradual transition from metal to ceramic phases along its thickness [1]. The effective properties characterizing FGM can be adjusted to suit specific requirements in diverse technical applications due to the adjustable gradation of the composition of

FGM. There are fewer stress discontinuities in FGM since the material properties change gradually and smoothly across the thickness and interlaminar stress discontinuities are eliminated [2].

The nonlinear free vibration has garnered lot of attention in recent years because linear model cannot represent actual the structural behaviour of the FGM plate [3–5]. The understanding of the large amplitude free flexural vibration behaviour of an FGM plate has got many technological applications, especially in aircraft panels. When a plate structure has got deflections comparable to its thickness, it develops significant geometrical nonlinearities, thus in-plane normal stresses may occur. Because the large amplitude vibrations cause in-plane stretching of the plate, these in-plane normal stresses are tensile in nature. They increase the plate stiffness. The resulting additional stiffening of the FGM plate causes resonance frequencies to rise and mode shapes to change.

Because this is a relatively new field, there is a shortage of published works on nonlinear forced and free vibrations of FGM plates, with the bulk of existing literature focused on linear problems. Finite element models (FEM) and theoretical formulations aimed at both dynamic and static analyses of functionally graded material plates, utilizing third-order shear deformation theory, were presented by Reddy [6]. Vel and Batra [7] provided a 3D analytical solution addressing the forced and free vibrations of simply supported rectangular FGM plates. Their approach employed the power series method to resolve the governing equations through appropriate displacement functions that adhere to the specified boundary conditions. Efraim and Eisenberger [8] determined the exact free vibration frequencies and modes for thick annular FGM plates with variable thickness. The geometrically nonlinear behaviour of circular FGM plates subjected to mechanical and thermal loads were investigated by Gunes and Reddy [9], who employed the full Green–Lagrange strain tensor. Nonlinear partial differential equations were constructed by Chen et al. [10] for the vibration motion of initially strained FGM plates. The formulation for the nonlinear vibrational behaviour of functionally graded materials (FGM) under a general condition of arbitrary initial stresses (CLPT) was derived utilizing classical laminated plate theory. static analysis and free vibration of FGM plates was investigated by Talha and Singh [11] using modified HSDT kinematics. The fundamental equations were derived through the variational approach by analysing the stress-free boundary conditions present at both the top and bottom surfaces of the plate. In a temperature setting, forced and free vibration studies for initially strained FGM plates were investigated by Yang and Shen [12]. The analysis assumes material properties that vary with temperature, utilizing the formulations derived from Reddy's higher-order shear deformation theory that considers uniform temperature changes caused by thermal effects. Sundararajan et al. [13] used von-Karman assumptions to build a nonlinear formulation to investigate the free vibration characteristics exhibited by FGM plates affected by temperature. In their study, FEM and a direct iterative approach were adopted to solve Lagrange's equations of motion and create nonlinear governing equations

The nonlinear vibration of FGM plates with non-uniform starting loads was demonstrated by Chen [14]. By employing the Galerkin method, the governing nonlinear partial differential equations have been reformulated into ordinary nonlinear differential equations, and the Runge–Kutta method was adopted to determine linear and nonlinear frequencies. Parametric resonance of FGM rectangular plates under harmonic in-plane loading, were demonstrated by Ng et al. [15]. Research revealed that altering the power-law exponent, which governs the distribution of materials within the structures, affects the parametric resonance of FGM rectangular plates. Allahverdizadeh et al. [16] developed a semi-analytical method to analyze nonlinear forced and free axis-symmetric vibrations in thin circular FGM plates. The incorporation of geometric nonlinearity follows the von Karman approach, with the formulation being based on the kinematics derived from Classical Laminate Plate Theory. For the nonlinear free vibration behavior of FGM plates, Woo et al. [17] proposed an analytical solution. The governing equations for thin rectangular FGM plates were derived using the von-Karman theory for significant transverse deflection, with the solution obtained through mixed Fourier series analysis. Huang and Shen explored dynamic response and nonlinear vibration of FGM plates in hot settings [18]. The formulation of the equations relies on HSDT kinematics and a general von-Karman type equation, which takes temperature effects into consideration. Under transverse and in-plane stresses, Yang and Shen [19] adopted a semi-analytical approach for studying large

deflection as well as post-buckling responses of FGM rectangular plates. The kinematics of the CLPT are used to create the formulas. Praveen and Reddy [20] investigated the behavior of FGM plates through finite element methods that incorporate transverse shear strains, rotational inertia, and significant rotations, in accordance with the von-Karman theory. The gradation of properties is presumed to follow a power-law across the thickness, with a comparative analysis conducted on homogeneous isotropic plates. The theoretical approach used to model the structure significantly influences the accurate representation of the nonlinear behavior of functionally graded materials. The standard laminated plate theory, which assumes that the normal to the mid-plane remains perpendicular during deflections, may not be suitable for FGM plates, where the volume fractions of multiple materials vary continuously with position in a designated direction. This error stems from the failure to account for the transverse shear and normal strains of the plate. The first-order shear deformation theory and higher-order shear deformation theory may provide valuable insights for analysis due to the continuous changes in material properties. Mindlin's first-order shear deformation theory does not fulfill the requirement for a parabolic distribution of transverse shear strain through the thickness, which affects the accuracy of the shear correction factors in the FSDT solutions. Therefore, these factors must be integrated into the adjustments for transverse shear stiffness. Typically, in the kinematics of HSDT, in-plane displacements are represented as a cubic function of the thickness coordinate, while out-of-plane displacement is considered constant.

In order to ensure the accountability of normal strain and its derivative in calculating transverse shear stresses, the kinematics of the structural model presumes a cubic variation of in-plane displacement across the full thickness, while the transverse displacement is assumed to vary quadratically. Researchers have focused on advancing higher-order shear deformation theory to gain insights into the mechanical behavior of constructions utilizing FGM [21, 22]. In this context, the analysis of geometrically nonlinear free flexural vibrations of FGM plates, employing higher-order shear deformation theory with geometric nonlinearity in the Green–Lagrange framework, is essential for accurately examining the responses of the FGM structure. The findings from the literature review reveal a notable deficiency in the available research concerning the nonlinear free vibration analysis of functionally graded plates that apply higher-order shear deformation theory kinematics, especially in relation to geometric nonlinearity within the Green–Lagrange sense. The goal of the presented study was to develop a novel HSDT approach with such a shear deformation function that it can accurately model the large amplitude free vibration behavior of the plate incorporating geometric nonlinearity. A simple nonlinear C^0 continuous isoparametric FE is presented and the obtained findings were compared to literature reports. The comprehensive parametric study has illustrated the variation of nonlinear fundamental frequencies with amplitude ratios for various boundary conditions, volume fraction indices, amplitude ratios, aspect ratios, and thickness ratios.

THEORETICAL FORMULATION

Geometric configuration of the FGM plate

The FGM plate consist of single layer of FGM with length a, breadth b, and a uniform thickness t. Figure 1 illustrates the geometry of a skew functionally graded material plate, which features a gradual variation in metal and ceramic compositions from the top to the bottom surface. The upper surface, located at Z (h/2), is predominantly composed of ceramic, while the lower surface at Z (-h/2) is primarily metal. The coordinates x, y, and z represent the in-plane and thickness directions, respectively. The skew angle is measured clockwise from the y-axis.

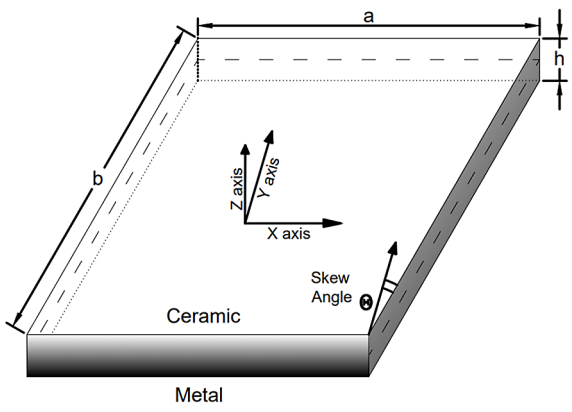

Figure 1. The geometry of the skew functionally graded plate

Material homogenization scheme

The material behaviour is considered to be linear elastic for small strains and large displacements. The composition of FGM is non-uniform and FGM constituents, unlike alloys or other chemical combinations, retain their mechanical properties. However, the gradual variation of the ceramic and metallic phases along the plate's thickness allows the use of various material homogenization schemes which can predict the mechanical properties of FGM at a particular depth. In Equation 1 the mechanical properties of ceramic P_c and metal P_m are employed to calculate the effective properties of plate material, e.g. Young's modulus E and density ρ. The Vc(z) given in Equation 2 constitutes the volume fraction of the ceramic and n corresponds to the volume fraction index, whereas material variation is described via power law distribution. The aforementioned power-law theory calculates a simple rule of mixtures (RM) that is utilized to determine the effective mechanical properties of a ceramic–metal graded plate. The RM only applies in the thickness direction.

$$P(z) = P_m + (P_C - P_m) \cdot V_C\,(z) \tag{1}$$

$$V_c\,(z) = \{1/2 + z/h\}^n \tag{2}$$

Displacement fields

Figure 1 shows that the material coordinates originate in the centroid of the plate. The kinematics of HSDT that has been proposed incorporates a hybrid hyperbolic shape function for in-plane displacements, thereby ensuring an accurate estimation of the transverse shear effects in the mathematical model. The displacement fields are described in Equation 3–5. The hybrid hyperbolic shape function which ensures the parabolic shear strain profile and removes the requirement of calculating the shear correction factor is described in Equation 6.

$$u(x,y,z) = u_0(x,y) - z\frac{\partial w}{\partial x} - f_z\phi_{sx}(x,y) \tag{3}$$

$$v(x,y,z) = v_0(x,y) - z\frac{\partial w}{\partial y} - f_z\phi_{sy}(x,y) \tag{4}$$

$$w(x,y,z) = w_0(x,y) \tag{5}$$

$$f_z = \frac{4*z^3}{3\cdot h^2\cdot \cosh\,(1)^2} - \frac{h}{2}tanh\left\{\frac{2\cdot z}{h}\right\} \tag{6}$$

The first-order derivatives produce second-order derivative terms in strain-displacement relationships and require C1 continuity (continuity of primary field variable and their first-order derivatives) in FE formulation. The algorithm of C1 continuity is very difficult and complex, hence the C1 continuity requirement must be avoided. The C1 continuity is reduced to C0 continuity which require the continuity of only primary field variables, by assigning new field variables to the first-order derivative terms expressed in Equation 7.

$$\theta_{bx} = \frac{\partial w}{\partial x}\,, \theta_{by} = \frac{\partial w}{\partial y} \tag{7}$$

These new unknown field variables cause artificial constraints in the governing equation of the plate. Thus, a penalty approach is used to enforce them into FE formulation. Equation 8–9 show the modified displacement fields for in-plane displacements .

$$u(x,y,z) = u_0(x,y) - z\cdot\theta_{bx}(x,y) - \\ -f_z\cdot\phi_{sx}(x,y) \tag{8}$$

$$v(x,y,z) = v_0(x,y) - z\cdot\theta_{by}(x,y) - \\ -f_z\cdot\phi_{sy}(x,y) \tag{9}$$

Strain-displacement relationship

The geometric non-linearity is incorporated in the strain-displacement relationships expressed in Equation 10 for FGM plate by using Green-Lagrange theory. The non-linear terms containing only transverse displacement are considered and geometric non-linearity due to in-plane displacements is ignored.

$$\begin{aligned}
\epsilon_{xx} &= \frac{\partial u_o}{\partial x} - z\frac{\partial\theta_{bx}}{\partial x} - f_z\frac{\partial\phi_{sx}}{\partial x} + \frac{1}{2}\left(\frac{\partial w_o}{\partial x}\right)^2 \\
\epsilon_{yy} &= \frac{\partial v_o}{\partial y} - z\frac{\partial\theta_{by}}{\partial y} - f_z\frac{\partial\phi_{sy}}{\partial y} + \frac{1}{2}\left(\frac{\partial w_o}{\partial y}\right)^2 \\
\gamma_{xy} &= \left\{\frac{\partial u_o}{\partial y} + \frac{\partial v_o}{\partial x}\right\} - z\left\{\frac{\partial\theta_{bx}}{\partial y} + \frac{\partial\theta_{by}}{\partial x}\right\} - \\
&\quad - f_z\left\{\frac{\partial\phi_{sx}}{\partial y} + \frac{\partial\phi_{sy}}{\partial x}\right\} + \frac{1}{2}\left(\frac{\partial w_o}{\partial x}\frac{\partial w_o}{\partial y}\right) \\
\gamma_{xz} &= \frac{\partial w_o}{\partial x} - \theta_{bx} + \frac{\partial f_z}{\partial z}\theta_{sx} \\
\gamma_{yz} &= \frac{\partial w_o}{\partial y} - \theta_{by} + \frac{\partial f_z}{\partial z}\theta_{sy}
\end{aligned} \tag{10}$$

The strains ϵ corresponding to ϵ_{xx}, ϵ_{yy} and γ_{xy} and transverse shear strain terms γ representing γ_{xz} and γ_{yz} given in Equation 10 terms can be rewritten in simplified form in Equation 11–12. Here [B] is differential operator matrix and [H] is thickness coordinate matrix.

$$\epsilon = [B^b][H^b]\{\delta\} + \frac{1}{2}[A^{nl}][G^{nl}][H^{nl}]\{\delta\} \tag{11}$$

$$\gamma = [B^s][H^s]\{\delta\} \tag{12}$$

Constitutive relationship

Equation 13 delineates the constitutive relationship that governs the relationship between stresses and strain in the context of the FGM plate domain. The modulus of elasticity E(z) and Poisson ratio υ(z) are calculated using RM for estimating $Q_{11} = Q_{22} = E(z)/(1-\upsilon(z)^2)$, $Q_{12} = E(z)\,\upsilon(z)/(1-\upsilon(z)^2)$ and $Q_{33} = Q_{44} = Q_{55} = E(z)/2(1+\upsilon(z))$. Further, $Q^b = [Q_{ij}]$ with i,j = 1,2,3 and $Q^s = [Q_{ij}]$ with i,j = 4,5.

$$\begin{bmatrix}\sigma_{xx}\\ \sigma_{yy}\\ \tau_{xy}\\ \tau_{xz}\\ \tau_{yz}\end{bmatrix} = \begin{bmatrix}Q_{11} & Q_{12} & 0 & 0 & 0\\ Q_{12} & Q_{22} & 0 & 0 & 0\\ 0 & 0 & Q_{33} & 0 & 0\\ 0 & 0 & 0 & Q_{44} & 0\\ 0 & 0 & 0 & 0 & Q_{55}\end{bmatrix} \cdot \begin{bmatrix}\epsilon_{xx}\\ \epsilon_{yy}\\ \gamma_{xy}\\ \gamma_{xz}\\ \gamma_{yz}\end{bmatrix} \tag{13}$$

Strain energy of the FGM plate

Equation 14 can be used to calculate the strain energy of the FGM plate. Putting the values of ϵ and γ into Equation 14, we get expression of strain energy presented in Equation 15.

$$U = \frac{1}{2}\int \epsilon^T\, \sigma\, \partial V + \frac{1}{2}\int \gamma^T \tau\, \partial V \tag{14}$$

$$U = \frac{1}{2}\int \left\{ \begin{array}{c} \{\delta\}^T[B^b]^T[D^b][B^b]\{\delta\} + \\ +\{\delta\}^T[B^s]^T[D^s][B^s]\{\delta\} + \\ +\frac{1}{2}\{\delta\}^T[B^b]^T[D^{nl1}][A^{nl}][G^{nl}]\{\delta\} + \\ +\{\delta\}^T[G^{nl}]^T[A^{nl}]^T[D^{nl2}][B^b]\{\delta\} + \\ +\frac{1}{2}\{\delta\}^T[G^{nl}]^T[A^{nl}]^T[D^{nl3}][A^{nl}][G^{nl}]\{\delta\} \end{array} \right\} \partial x \partial y \tag{15}$$

Similarly, Equation 16 defines the kinetic energy of the FGM plate, where u = $[H^m]$*δ represent the displacements.

$$\begin{aligned} T &= \frac{1}{2}\iint \rho \cdot (\dot{u})^2\, \partial x \partial y\, \partial z = \\ &= \frac{1}{2}\int \{\dot{\delta}\}^T\, D^m \{\dot{\delta}\} \partial x \partial y \end{aligned} \tag{16}$$

The expression of the D^b, D^s, D^m, D^{nl1}, D^{nl2} and D^{nl3} are presented in Equation 17.

Governing equations

By implementing the principle of virtual work on the Lagrangian (L), the governing differential equation of motion can be obtained, as expressed in Equation 18. The given equation is derived by principle which is a generalization of principal of virtual work. The artificial constraints which have been imposed for maintaining C0 continuity in the FE formulation is taken into consideration.

$$\begin{aligned} &\frac{\partial T}{\partial\{\dot{\delta}\}} + \frac{\partial U}{\partial\{\delta\}} + \\ &+ \frac{\partial}{\partial\{\delta\}}\int \frac{\gamma_c}{2}\left\{ \begin{array}{l} (\theta_{bx} - w_{0,x})^2 + \\ +(\theta_{by} - w_{0,y})^2 \end{array} \right\} \partial V = 0 \end{aligned} \tag{18}$$

FINITE ELEMENT FORMULATION

The FE formulation is developed by implementing nine-noded C0 continuity isoparametric elements. There are seven degrees of freedom (DOFs) per node namely $\{u_o, v_o, w_o, \theta_{bx}, \theta_{by}, \phi_{sx}, \phi_{sy}\}$. The geometry of the FGM plate domain and displacement fields can be interpolated using Lagrangian shape functions expressed in Equation 19.

The use of nine-noded elements allow us to use full-scale gauss quadrature integration scheme which improves the accuracy of the results to great extent.

$$\delta = \sum_{i=1}^{9} N_i \delta_i, x = \sum_{i=1}^{9} N_i x_i, y = \sum_{i=1}^{9} N_i y_i \tag{19}$$

Derivation of stiffness and mass matrix

When the expression of strain energy from Equation 15 and kinetic energy from Equation 16 is introduced into Lagrange equation of motion stated in Equation 18, the governing equation can be expressed in Equation 20. Here, M denotes the mass matrix, whereas K corresponds to the stiffness matrix containing the contribution from linear and nonlinear components i.e., $K = K_B + K_S + \{K_{NL1} + K_{NL2} + K_{NL3}\}$, and K_c is the stiffness

$$\begin{aligned} D^b &= \int_{-h/2}^{h/2} [H^b]^T[Q^b][H^b]\partial z,\; D^s = \int_{-h/2}^{h/2} [H^s]^T[Q^s][H^s]\partial z \\ D^{nl1} &= \int_{-h/2}^{h/2} [H^b]^T[Q^b][H^{nl}]\partial z, D^{nl2} = \int_{-h/2}^{h/2} [H^{nl}]^T[Q^b][H^b]\partial z \\ D^{nl3} &= \int_{-h/2}^{h/2} [H^{nl}]^T[Q^b][H^{nl}]\partial z\,,\; D^m = \int_{-h/2}^{h/2} \rho[H^m]^T[H^m]\partial z \end{aligned} \tag{17}$$

matrix resulting from artificial constraints needed for C0 continuity of FE formulation.

$$[M]\{\ddot{\delta}\} + ([K] + [K_c])\{\delta\} = 0 \tag{20}$$

Here M and K matrix are defined as follows:

$$\begin{aligned}
[M] &= \int N^T D^m N \partial x \partial y, \\
K_b &= \int [B^b]^T [D^b][B^b]\, \partial x \partial y, \\
K_s &= \int [B^s]^T [D^s][B^s] \partial x \partial y, \\
K_{nl1} &= \frac{1}{2}\int [B^b]^T [D^{nl1}][A^{nl}][G^{nl}]\, \partial x \partial y, \\
K_{nl2} &= \int [G^{nl}]^T [A^{nl}]^T [D^{nl2}][B^b] \partial x \partial y, \\
K_{nl2} &= \frac{1}{2}\int [G^{nl}]^T [A^{nl}]^T [D^{nl3}][A^{nl}][G^{nl}] \partial x \partial y
\end{aligned} \tag{21}$$

Solution procedure

The free vibration analysis is performed for the given FGM plate without considering the effect of geometric nonlinearity i.e., $K = K_B + K_S$. The relationship between acceleration and displacement for harmonic vibrations holds true and $\{\ddot{\delta}\} = -\omega^2\{\delta\}$. The effect of the artificial constraint is neglected and this that the Equation 20 will be reduced to Equation 22.

$$-\omega^2[M]\{\delta\} + [K]\{\delta\} = 0 \tag{22}$$

The Reyleigh iteration approach is used to tackle this eigenvalue problem. Initially, Equation 22 is solved, with all nonlinear terms [K_{nl1}], [K_{nl2}], and [K_{nl3}] set to zero by utilizing a zero eigenvector, thereby yielding the linear response with a normalized first mode. The mode shape representing the transverse displacement of the FGM plate obtained from linear fundamental frequency (ω_L) is then scaled to achieve the desired amplitude ratio w/h (where w denotes the maximum transverse displacement and h signifies the plate thickness). The scaled-up transverse displacement vector [w_o] is used to obtain nonlinear stiffness matrices [K_{nl1}], [K_{nl2}], and [K_{nl3}]. The nonlinear fundamental frequency is derived for K having non-linear stiffness and the corresponding eigenvectors are calculated to update the non-linear stiffness matrices for the next iteration. This procedure is repeated until the eigenvalues from the next two iterations fall within the specified tolerance limit of less than $< 10^{-3}$. The convergence is expected to occur at the tolerance limit, and the converged frequency is considered as the FGM plate's nonlinear frequency (ω_{NL}). The frequency ratio (ω_{NL}/ω_L) corresponding to given amplitude ratios (w/h) are compared with existing literature for validation.

RESULTS AND DISCUSSION

This study investigated the effect of geometric nonlinearity in free flexural vibration behaviour of FGM plates. The FE model developed from the Lagrange's equation of motion based on proposed HSDT kinematics is used to calculate the frequency and mode shapes. The Green-Lagrange theory was added into the formulation to account for the geometric nonlinearity due to large amplitude free vibrations in the plate. There has been a computer program created using MATLAB 9.6.0 (R2019a) environment. To evaluate the accuracy of the algorithm, its results are compared against established findings in the literature. The current integration scheme uses full integration scheme with 3X3 gauss quadrature rule of integration to compute the stiffness and mass matrix accurately. The material is assumed to behave elastically and the non-linearity of the material behaviour has been ignored. The convergence of mesh size is studied to find the optimum mesh size for the application even though such restrictions are not imposed by the FE model. In order to validate the efficacy of the model, the converged results are contrasted with previous findings. The comprehensive parametric studies are performed on the model to explore the behaviour of the FGM plate for various boundary conditions, side-to-thickness ratios, aspect ratios, skewness, and material properties. The boundary conditions for the FGM plate are described as follows: -

1. All sides simply supported (SSSS):

$$v, w, \theta_x \text{ and } \phi_x \text{ are } 0 \text{ at } x = 0, a$$

$$u, w, \theta_y \text{ and } \phi_y \text{ are } 0 \text{ at } y = 0, b$$

2. All sides clamped (CCCC):

$$u, v, w, \theta_x, \phi_x\ \theta_y \text{ and}$$

$$\phi_y \text{ are } 0 \text{ at } x = 0, a \text{ and } y = 0, b$$

3. Two sides simply supported two sides clamped (SCSC):

$$v, w, \theta_x \text{ and } \phi_x \text{ are } 0 \text{ at } x = 0, a$$

$$u, v, w, \theta_x, \phi_x\ \theta_y \text{ and } \phi_y \text{ are } 0 \text{ at } y = 0, b$$

Table 1 presents the material properties of the metallic and ceramic materials used to create FGM composite. The temperature T = 300 K is

Table 1. Mechanical properties of the metal and ceramic at T = 300 K

Material	E (GPa)	ρ (kg/m^3)	υ	
Metal	Aluminum (Al)	70	2707	0.3
	Titanium alloy (Ti–6Al–4V)	105.7	4429	0.298
	Stainless steel (SUS304)	207.78	8166	0.28
Ceramic	Alumina (Al_2O_3)	380	3800	0.3
	Zirconia (ZrO_2)	151	3000	0.30
	Silicon nitride (Si_3N_4)	427	3210	0.28

used as reference temperature for the values of modulus of elasticity (E), density (ρ) and Poisson ratio (υ) presented in the Table 1.

The accuracy of the current FE formulation, which utilizes the proposed Higher-Order Shear Deformation Theory alongside a general von-Karman geometric nonlinearity, is confirmed through a comparison of results with existing studies [23]. A study of the mesh convergence is also offered. The analysis of free vibrations is conducted on an FGM square plate that is simply supported along all four edges. The study considers various amplitude ratios (w_{max}/h) with a volume fraction index of n = 2. The plate is square with sides a = b = 0.2. The maximum deflection at the center of the plate is denoted as w_{max}. The FGM plate is composed of titanium alloy (Ti–6Al–4V) for the metal component and zirconia (ZrO_2) for the ceramic component. As shown in Table 2, the results were calculated using the frequency ratio (ω_{nl}/ω_l) with various mesh divisions. This demonstrates that the accuracy of the solution and the rate of convergence with mesh refinement are satisfactory for the frequency ratio (ω_{nl}/ω_l) across varying amplitude ratios (w_{max}/h). The convergence leads to the conclusion that a 10X10 mesh is enough for nonlinear analysis. The present study incorporates geometric nonlinearity through the Green–Lagrange theory, addressing all higher-order nonlinear strain components. Nevertheless, a thorough investigation has shown that the von-Karman geometric nonlinearity yields reasonably accurate results up to (w_{max}/h) = 0.6, which is omitted here for simplicity.

The study examined the nonlinear free vibration time periods of a square (a/h = 10) FGM plate composed of stainless steel (SUS304) and silicon nitride (Si_3N_4) across various volume fraction indices. The variations in nonlinear time periods for a simply supported FGM plate corresponding to different volume fraction indices are shown in Table 3.The analysis is done for the amplitude ratios 0.2, 0.6 and 1.0. Non-dimensional linear period described in Equation 23 is calculated and it is compared with the non-linear period by Chen [21]. It can be seen that the higher amplitude ratios result in lower time periods of vibrations. A reduced index value for the volume fraction suggests a more significant rise in the ceramic volume fraction from the base layer of the FGM plate.

$$T = T_o * \sqrt{\{\pi^2 E/12(1-\nu^2)\rho a^2\}} \qquad (23)$$

The influence of varying thickness ratios (a/h), from thick to thin plates, on the volume fraction index n is shown in Table 4. The square FGM plate composed of Ti–6AL–4V/ZrO_2 is simply supported on all sides with the volume fraction index n defined as 1As the thickness ratio increases, the frequency ratio (ω_{nl}/ω_l) decreases, with more

Table 2. Fundamental nonlinear frequency ratios ω_{NL}/ω_L for different amplitude ratios of a square SSSS (Ti–6AL–4V/ZrO_2) FGM plate with varying mesh sizes

Mesh size	Amplitude Ratio (w_{max}/h)				
	0.2	0.4	0.6	0.8	1.0
Ref [20]	1.0455	1.1409	1.2765	1.4244	1.6055
Present (4 × 4)	1.0451	1.1386	1.2702	1.4301	1.6098
Present (6 × 6)	1.0451	1.1387	1.2708	1.4314	1.6115
Present (8 × 8)	1.0451	1.1388	1.271	1.4316	1.6101
Present (10 × 10)	1.0451	1.1388	1.271	1.4317	1.6075
Present (12 × 12)	1.0451	1.1388	1.271	1.4318	1.6067

Table 3. Comparison of nonlinear periods for different volume fraction indices (n) of simply supported (SUS304/ Si_3N_4) FGM plates (a/b = 1, a/h = 10)

n	Linear period	Amplitude ratio (w_{max}/h)					
		0.2		0.6		1.0	
		Ref [21]	Present	Ref [21]	Present	Ref [21]	Present
10	11.008	10.703	12.3351	8.911	10.3013	7.034	8.1677
5	10.69	10.422	11.7132	8.6767	9.7484	6.845	7.7335
2	9.959	9.695	10.6014	8.045	8.7689	6.331	6.9411
1	9.136	8.897	9.5427	7.354	7.88	5.772	6.2233
0.5	8.231	8.011	8.4298	6.609	6.9816	5.187	5.5098
0.2	7.236	7.031	7.2355	5.811	6.032	4.562	4.7655
0.1	6.741	6.547	6.6597	5.416	5.5735	4.257	4.4077
Ceramic	6.097	5.915	5.9286	4.901	4.9878	3.855	3.9513

significant variations observed at lower thickness ratios compared to higher ones, meaning that current HSDT is better suited to thick plates, whereas higher-order terms should be considered in the analysis of thick plates.. Furthermore, it is evident that the frequency ratio expands in conjunction with an increase in the amplitude ratio. The trends of the frequency ratios are disrupted at various places due to the presence of significant nonlinearity and they have been shown in bold. As a result, it can be argued that analyzing geometric nonlinear systems in the Green–Lagrange theory is critical for closely monitoring structural reaction.

The influence that boundary conditions have on the nonlinear frequency ratio (ω_{nl}/ω_l) was studied for SCSC square SUS304/ Si_3N_4 FGM plates. As shown in Table 5, the frequency ratio (ω_{nl}/ω_l) fluctuates in relation to the amplitude ratio (w_{max}/h). The results indicate that the frequency ratio increases with the volume fraction index n until it reaches a peak at n = 2, after which it decreases with further increases in n. Notably, the frequency ratio for a/h = 10 is higher than that for a/h = 20. Furthermore, the frequency ratio is positively correlated with the amplitude ratio, as larger amplitude vibrations lead to increased nonlinear frequencies. The influence of boundary conditions on the nonlinear frequency ratio (ω_{nl}/ω_l) was studied for CCCC square Al/ ZrO_2 FGM plates. Table 6 demonstrates how the frequency ratio (ω_{nl}/ω_l) varies with the amplitude ratio (w_{max}/h). The frequency ratio rises along with the volume fraction index n until it reaches a certain threshold, specifically at n = 2, after which it begins to decline with further increases in n. When comparing a/h = 20 to a/h = 10, the frequency ratio is higher for a/h = 10. Additionally, the frequency ratio grows with the amplitude ratio, because non-linear frequencies increase for large-amplitude vibrations.

The influence of gradation rate on the nonlinear free vibration can be tested by using two set of FGM material. One with Al/Al_2O_3 having E_c/E_m = 5.42 and other Al/ZrO_2 having E_c/E_m = 2.15. A higher E_c/E_m ratio results in a more significant change in material properties relative to thickness. The simply supported square plate with thickness ratio (a/h=10) was taken for the analysis. The nonlinear free vibration analysis was performed for various n and amplitude ratios. It can

Table 4. Influence of varying thickness ratios (a/h) with the volume fraction index n for (Ti–6AL–4V/ZrO_2) FGM plates consistent with SSSS boundary condition

a/h	Amplitude ratio (w_{max}/h)				
	0.5	1.0	1.6	2.0	2.5
5	1.2448	1.5238	1.787	1.7929	**1.7196**
15	1.2196	1.6312	1.6773	**1.697**	2.1885
25	1.2175	1.6243	1.675	1.7818	1.8321
50	1.2165	1.6206	**1.8395**	1.7811	1.68
100	1.2161	1.6194	**2.0462**	1.7117	1.6911

Table 5. Influence of volume fraction index n and thickness ratio on the fundamental nonlinear frequency ratio (ω_{nl}/ω_l) of a square SCSC (SUS304/Si_3N_4) FGM plate

a/h	n	Amplitude ratio (w_{max}/h)					
		0.4	0.8	1.2	1.6	2.0	2.4
10	0	1.057	1.2129	1.4355	1.5887	1.508	1.3085
	0.5	1.0683	1.2357	1.4683	1.5466	1.5503	1.4799
	1	1.0714	1.2405	1.4736	1.5403	1.5555	1.4844
	2	1.0707	1.2361	1.4642	1.5402	1.5528	1.4788
	5	1.0651	1.222	1.4411	1.5498	1.5423	1.4668
	10	1.0613	1.215	1.4314	1.5625	1.5334	1.4698
	20	1.0592	1.2126	1.4301	1.5725	1.5235	1.5094
20	0	1.0526	1.1977	1.4081	1.6487	1.5982	1.5279
	0.5	1.0633	1.2197	1.4403	1.6852	1.5523	1.5949
	1	1.0661	1.2239	1.4448	1.6885	1.5604	1.605
	2	1.0652	1.2188	1.4339	1.6747	1.5649	1.606
	5	1.0596	1.2042	1.4091	1.6442	1.585	1.5911
	10	1.0561	1.1976	1.4	1.6338	1.5992	1.573
	20	1.0542	1.1959	1.3999	1.6353	1.6033	1.5564

Table 6. Influence of volume fraction index n and thickness ratio on the fundamental nonlinear frequency ratio (ω_{nl}/ω_l) of a square CCCC (Al/ZrO_2) FGM plate

a/h	n	Amplitude ratio (w_{max}/h)					
		0.4	0.8	1.2	1.6	2.0	2.4
10	0	1.0421	1.1584	1.3274	1.4461	1.436	1.4549
	0.5	1.044	1.165	1.3402	1.4148	1.4379	1.4535
	1	1.0439	1.1649	1.34	1.4056	1.4316	1.4504
	2	1.0425	1.1597	1.3301	1.4032	1.4236	1.4435
	5	1.04	1.1507	1.3128	1.4123	1.4175	1.4371
	10	1.0394	1.1486	1.3085	1.421	1.4193	1.4398
	20	1.0398	1.1502	1.3116	1.4305	1.4241	1.4453
20	0	1.0389	1.1471	1.3067	1.496	1.4866	1.4621
	0.5	1.0407	1.1538	1.3198	1.5084	1.4418	1.4774
	1	1.0406	1.1534	1.3191	1.5037	1.436	1.4761
	2	1.039	1.1477	1.3079	1.4919	1.4371	1.4699
	5	1.0364	1.1381	1.289	1.4694	1.4542	1.4591
	10	1.0359	1.1363	1.2853	1.4644	1.4701	1.4558
	20	1.0364	1.1383	1.2894	1.4706	1.4798	1.4569

be observed that the variation in amplitude ratio is more drastic for higher E_c/E_m Al/Al_2O_3 FGM plate. This implies that the effect of rate of change of gradation influences the nonlinear free vibrations of the plate.

The relationship between varying aspect ratios (a/b) and the frequency ratio (ω_{nl}/ω_l) for multiple amplitude ratios is depicted in Table 8. The square Al/ZrO_2 FGM plate is simply supported on all sides, with the volume fraction index n taken as 1.The frequency ratio (ω_{nl}/ω_l) increase as the aspect ratio increases, attaining the maximum value near square geometry and then it decreases with higher aspect ratios. The changes are more prominent for smaller aspect ratios. The changes are almost symmetric about square geometry for plates subjected to smaller amplitudes ratios. For higher amplitude ratios, the maximum frequency ratio is observed for plates with aspect ratio smaller than unity. The impact of skew angles on the stiffening

Table 7. The effect of gradation rate on the fundamental nonlinear frequency ratio (ω_{nl}/ω_l) of a square simply supported the FGM plate

FGM	n	Amplitude ratio (w_{max}/h)					
		0.5	1	1.4	1.8	2.4	3.0
Al/ZrO_2	0	1.1615	1.5535	1.6369	1.7055	2.3157	2.484
	0.5	1.2195	1.6432	1.6338	1.6585	2.2366	2.3986
	1	1.2357	1.6615	1.6353	1.6567	2.1832	2.3459
	2	1.2346	1.6498	1.6257	1.6492	2.1376	2.3009
	5	1.2111	1.6051	1.6157	1.6475	2.1338	2.2999
	10	1.1922	1.5775	1.6259	1.671	2.1707	2.3404
Al/Al_2O_3	0	1.1614	1.2108	1.6183	1.5684	1.7022	2.0646
	0.5	1.2614	1.5532	1.5831	1.5811	1.6317	1.9504
	1	1.299	1.7048	1.637	1.6038	1.6053	1.9019
	2	1.3079	1.7077	1.6471	1.7032	1.633	1.9507
	5	1.2729	1.6634	1.6224	1.6941	2.3037	2.0364
	10	1.2388	1.6552	1.5742	1.7459	2.1733	2.4807

Table 8. The influence of aspect ratio on the fundamental nonlinear frequency ratio (ω_{nl}/ω_l) of a square simply supported the FGM plate

a/b	Amplitude ratio (w_{max}/h)				
	0.5	1.0	1.4	1.8	2.4
0.5	1.3622	1.384	1.4905	1.612	1.7104
0.75	1.3117	1.7811	1.5815	1.8033	2.173
1	1.299	1.7077	1.6224	1.7459	2.0646
1.5	1.3305	1.4479	1.5399	1.6546	1.8051
2	1.369	1.3161	1.3576	1.3919	1.4596

characteristics of a simply supported FGM plate was investigated. The RM scheme was employed to define the mechanical properties characterizing the Al/Al_2O_3 FGM plate. A nonlinear free vibration analysis was conducted for both thin and thick skew FGM plates, all with edges of equal length. The fundamental frequency of linear free vibration is compared with the findings of authors [24] for an isotropic ceramic phase across various plate thicknesses and skew angles. As shown in Table 9, an increase in the skew angle results in a general stiffening effect on displacement values, with larger skew angles corresponding to lower frequency ratios. Overall trends of larger

Table 9. Influence of the skewness angles on the fundamental frequency ratios (ω_{nl}/ω_l) of the simply supported FGM plate

a/h	Skew	Ref	Present	Amplitude ratio (w_{max}/h) for n = 1			
	Angle(θ)	ω_{Linear}	ω_{Linear}	0.2	0.5	1	1.5
5	0°	1.7661	1.7194	1.1013	1.3362	1.4971	1.6866
	15°	1.856	1.8113	1.097	1.3249	1.4522	1.6324
	30°	2.1719	2.1361	1.0855	1.2931	1.3877	1.5597
	45°	2.9129	2.901	1.0694	1.2452	1.3244	1.3388
10	0°	1.9311	1.9008	1.0944	1.3076	1.7132	1.612
	15°	2.0379	2.0081	1.0907	1.2981	1.6767	1.5737
	30°	2.4195	2.3964	1.0803	1.271	1.5965	1.5256
	45°	3.3548	3.3605	1.0655	1.2304	1.4697	1.4531

Table 10. Effect of the skewness angles on the fundamental frequency ratios (ω_{nl}/ω_l) of the clamped Al/Al_2O_3 FGM plate

a/h	Skew	Amplitude ratio (w_{max}/h) for n = 1					
	Angle (θ)	0.2	0.5	1.0	1.5	2.5	2.0
5	0	1.0165	1.0974	1.3201	1.3454	1.5007	1.5161
	15	1.0168	1.0992	1.3117	1.3415	1.4756	1.5112
	30	1.018	1.106	1.2659	1.3309	1.4328	1.4697
	45	1.021	1.1235	1.2316	1.3534	0.975	1.3366
10	0	1.0126	1.0757	1.2741	1.3957	1.4688	1.4225
	15	1.0127	1.0761	1.2754	1.379	1.4747	1.4164
	30	1.0129	1.0776	1.2804	1.3409	1.483	1.3982
	45	1.0136	1.0814	1.2923	1.3113	1.4877	1.3783

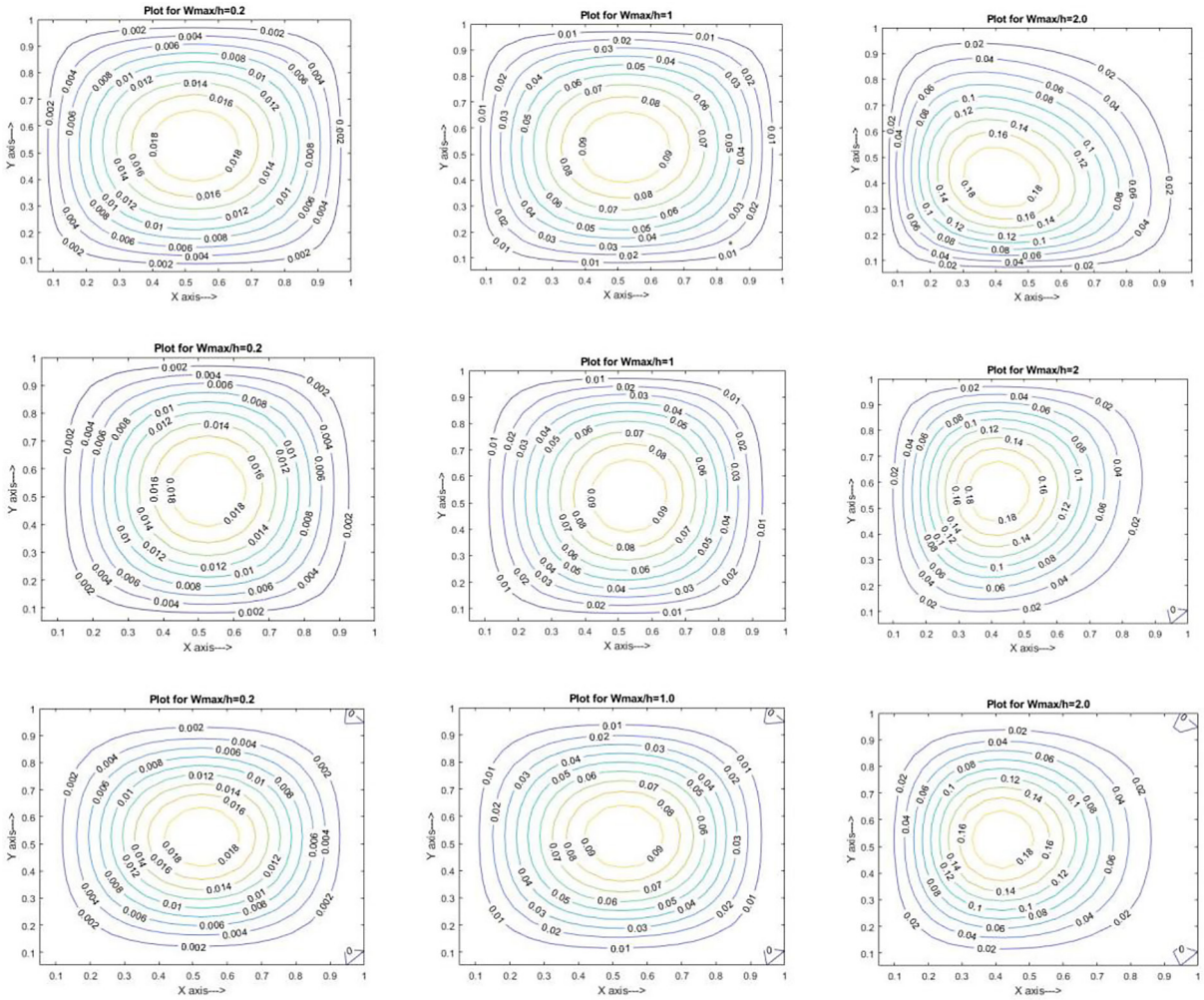

Figure 2. The mode shape distribution of Al/Al_2O_3 FGM plate for various boundary conditions and amplitude ratios

amplitude ratio resulting in larger nonlinear fundamental frequencies maintained. The fundamental frequency ratio (ω_{nl}/ω_l) decreases with thickness of the plate corresponding to better flexural strength of thicker plates.

$$\omega_{Linear} = \omega_o \cdot \sqrt{\frac{12(1-v_c^2)\rho_c a^2 b^2}{\pi^4 h^2 E_c}} \qquad (24)$$

By securing the edges of the skew FGM plate, any complexities associated with uncertainties

regarding rotational displacement at the slanted edges are eliminated. The clamped skew plate with all sides having equal length and thickness ratio (a/h = 5, 10) for n = 1 is for nonlinear free vibration. The frequency ratios are (ωnl/ωl) estimated for various the skew angle. The RM method was employed to describe the effective mechanical properties characterizing the Al/Al_2O_3 FGM plate. When edges are clamped, the displacement is minimized due to the restriction of angular displacements at those edges. This reduction in movement lessens the effects of geometric nonlinearity, yielding smaller frequency ratios. The increase in skewness reduces the deflection and conversely the frequency ratios are (ωnl/ωl) as shown in the Table 10. The effect of nonlinearity is more pronounced in thinner plates as compared to thicker plates.

The mode redistribution phenomena for Al/Al_2O_3 FGM plate with a/h =10 is shown in Figure 2 for SSSS,SCSC and CCCC boundary conditions. For larger amplitude ratios, the mode shapes start redistributing and shifting as can be seen in contour plot of the transverse displacement mode shape of the plate. This phenomenon of mode distribution, namely the mode shape of the plate shift towards one corner/edge of the plate for higher modes of vibration is quite unique and demonstrates the behaviour of plate subjected to large amplitude vibrations. The shifting is towards one corner for simply supported plate. The clamped plate observes shifting to an edge and clamped-simply supported plate observes the combination of shifting towards edge as well as towards a corner.

CONCLUSIONS

The present HSDT has been used to study the geometrical nonlinear free flexural vibration analysis of the FGM plate. The FE model was developed from the proposed HSDT and green-lagrange theory for non-linear analysis. The algorithm for calculating the non-linear and linear frequency ratios using the Rayleigh iteration method is developed in MATLAB, utilizing nine-noded C0 continuous isoparametric Lagrangian elements, each with seven degrees of freedom per node. To ensure the accuracy of the current formulation, convergence and validation studies were conducted. The numerical findings for different combinations of boundary conditions, volume fraction indices, thickness ratios, and aspect ratios were provided. The findings underscore the critical role and requirement for higher-order nonlinear terms. The main observations can be highlighted as follows:

- As the amplitude ratio increase, there is an increase in nonlinear free vibration frequencies.
- Increasing ceramic volume fraction improves the stiffness and decreases the nonlinear frequencies.
- The effect of higher rate of change in mechanical properties of ceramic to metallic phase produces drastic changes in frequency ratios of the plate.
- The effect of fundamental frequency ratio increases along with thickness ratios.
- The fundamental frequency ratio shows maximum value for square geometry irrespective of amplitude ratios.
- The clamped plate shows lesser values of fundamental frequency ratio compared to the simply supported plates.
- The influence of skewness of the plate has overall stiffening effect and it shows lesser values of fundamental frequency ratio.
- The modal redistribution happens for large amplitude ratios and mode shape shifts to corner for simply supported plate and it shifts to edges for clamped plates.

The algorithm can be implemented for different non-power-law distributions for material properties (e.g., exponential, sigmoid, or arbitrary functions) to better reflect real-world manufacturing capabilities or design requirements. The current formulation can be implemented in plates with material properties varying in two or three directions (e.g., in-plane grading, or combined thickness and in-plane grading). The effect of porosity, variable thickness profiles (e.g., tapered, stepped) and curved shell structures which have more complex geometries and find extensive use in aerospace and other industries can be incorporated for analysis. The nonlinear free vibration of FGM plates can be extended to study of its behavior under different thermal environments and moisture absorption conditions which lead to hygro-thermo-mechanical coupling. Better higher-order shear deformation theories which might offer better accuracy for very thick plates or specific loading conditions, while still maintaining computational efficiency, can be explored.

REFERENCES

1. Koizumi, M. F. G. M. FGM activities in Japan. Composites Part B: Engineering 1997, 28(1–2), 1–4. https://doi.org/10.1016/S1359-8368(96)00016-9
2. Koizumi, M., Nino, M. Overview of FGM research in Japan. Mrs Bulletin 1995, 20(1), 19–21. https://doi.org/10.1557/S0883769400048867
3. Ansari M. I., Kumar A., Fic S., Barnat-Hunek D. Flexural and Free Vibration Analysis of CNT-Reinforced Functionally Graded Plate. Materials 2018, 11, 2387; https://doi.org/doi:10.3390/ma11122387
4. Singh J., Kumar A., Szafraniec M., Barnat-Hunek D., Sadowska-Buraczewska B. Static analysis of skew functionally graded plate using novel shear deformation theory. Materials 2022, 15, 4633. https://doi.org/10.3390/ma15134633
5. Anish, A. Chaubey , A. Kumar, B. Kwiatkowski, D. Barnat-Hunek, M. K. Widomski, Bi-Axial Buckling of Laminated Composite Plates Including Cutout and Additional Mass. Materials 2019, 12(11), 1750; https://doi.org/10.3390/ma12111750
6. Reddy, J. Analysis of functionally graded plates. International Journal for numerical methods in engineering 2000, 47(1–3), 663–684. https://doi.org/10.1002/(SICI)1097-0207(20000110/30)47:1/3<663::AID-NME787>3.0.CO;2-8
7. Vel, S. S., Batra, R. C. Three-dimensional exact solution for the vibration of functionally graded rectangular plates. Journal of Sound and Vibration 2004, 272(3–5), 703–730. https://doi.org/10.1016/S0022-460X(03)00412-7
8. Efraim, E., Eisenberger, M. Exact vibration analysis of variable thickness thick annular isotropic and FGM plates. Journal of Sound and Vibration 2007, 299(4–5), 720–738. https://doi.org/10.1016/j.jsv.2006.06.068
9. Gunes, R., Reddy, J. N. Nonlinear analysis of functionally graded circular plates under different loads and boundary conditions. International Journal of Structural Stability and Dynamics 2008, 8(1), 131–159. https://doi.org/10.1142/S0219455408002582
10. Chen, C. S., Chen, T. J., Chien, R. D. Nonlinear vibration of initially stressed functionally graded plates. Thin-walled structures 2006, 44(8), 844–851. https://doi.org/10.1016/j.tws.2006.08.007
11. Talha, M., Singh, B. Static response and free vibration analysis of FGM plates using higher order shear deformation theory. Applied Mathematical Modelling 2010, 34(12), 3991–4011. https://doi.org/10.1016/j.apm.2010.03.034
12. Yang, J., Shen, H. S. Vibration characteristics and transient response of shear-deformable functionally graded plates in thermal environments. Journal of Sound and Vibration 2002, 255(3), 579–602. https://doi.org/10.1006/jsvi.2001.4161
13. Sundararajan, N., Prakash, T., Ganapathi, M. Nonlinear free flexural vibrations of functionally graded rectangular and skew plates under thermal environments. Finite Elements in Analysis and Design 2005, 42(2), 152–168. https://doi.org/10.1016/j.finel.2005.06.001
14. Chen, C. S. Nonlinear vibration of a shear deformable functionally graded plate. Composite Structures 2005, 68(3), 295–302. https://doi.org/10.1016/j.compstruct.2004.03.022
15. Ng, T. Y., Lam, K. Y., Liew, K. M. Effects of FGM materials on the parametric resonance of plate structures. Computer Methods in Applied Mechanics and Engineering 2000, 190(8–10), 953–962. https://doi.org/10.1016/S0045-7825(99)00455-7
16. Allahverdizadeh, A., Naei, M. H., Bahrami, M. N. Nonlinear free and forced vibration analysis of thin circular functionally graded plates. Journal of sound and vibration 2008, 310(4–5), 966–984. https://doi.org/10.1016/j.jsv.2007.08.011
17. Woo, J., Meguid, S. A., Ong, L. S. Nonlinear free vibration behaviour of functionally graded plates. Journal of sound and vibration 2006, 289(3), 595–611. https://doi.org/10.1016/j.jsv.2005.02.031
18. Huang, X. L., Shen, H. S. Nonlinear vibration and dynamic response of functionally graded plates in thermal environments. International Journal of Solids and Structures 2004, 41(9–10), 2403–2427. https://doi.org/10.1016/j.ijsolstr.2003.11.012
19. Yanga, J., Shen, H. S. Non-linear analysis of functionally graded plates under transverse and in-plane loads. International Journal of Non-Linear Mechanics 2003, 38(4), 467–482. https://doi.org/10.1016/S0020-7462(01)00070-1
20. Praveen, G. N., Reddy, J. N. Nonlinear transient thermoelastic analysis of functionally graded ceramic-metal plates. International journal of solids and structures 1998, 35(33), 4457–4476. https://doi.org/10.1016/S0020-7683(97)00253-9
21. Matsunaga, H. Free vibration and stability of functionally graded plates according to a 2-D higher-order deformation theory. Composite structures 2008, 82(4), 499–512. https://doi.org/10.1016/j.compstruct.2007.01.030
22. Mindlin, R. Influence of rotatory inertia and shear on flexural motions of isotropic, elastic plates 1951. https://doi.org/10.1115/1.4010217
23. Talha, M., Singh, B. N. (2011). Large amplitude free flexural vibration analysis of shear deformable FGM plates using nonlinear finite element method. Finite Elements in Analysis and Design 2011, 47(4), 394–401. https://doi.org/10.1016/j.finel.2010.11.006
24. Zhao, X., Lee, Y. Y., Liew, K. M. Free vibration analysis of functionally graded plates using the element-free kp-Ritz method. Journal of sound and Vibration 2009, 319(3–5), 918–939. https://doi.org/10.1016/j.jsv.2008.06.025